Estimation of potassium levels in hemodialysis patients by T wave nonlinear dynamics and morphology markers

Hassaan A. Bukhari [a,b,c,d,*], Carlos Sánchez [a,b], Sabarathinam Srinivasan [a,b], Flavio Palmieri [b,e], Mark Potse [c,d], Pablo Laguna [a,b], Esther Pueyo [a,b]

[a] BSICoS group, I3A Institute, University of Zaragoza, IIS Aragón, Zaragoza, Spain
[b] CIBER en Bioingeniería, Biomateriales y Nanomedicina (CIBER-BBN), Zaragoza, Spain
[c] Carmen team, Inria Bordeaux – Sud-Ouest, Talence, France
[d] University of Bordeaux, IMB, UMR 5251, Talence, France
[e] Centre de Recerca en Enginyeria Biomèdica, Universitat Politècnica de Catalunya, Barcelona, Spain

ARTICLE INFO

ABSTRACT

Objective: Noninvasive screening of hypo- and hyperkalemia can prevent fatal arrhythmia in end-stage renal disease (ESRD) patients, but current methods for monitoring of serum potassium ($[K^+]$) have important limitations. We investigated changes in nonlinear dynamics and morphology of the T wave in the electrocardiogram (ECG) of ESRD patients during hemodialysis (HD), assessing their relationship with $[K^+]$ and designing a $[K^+]$ estimator.
Methods: ECG recordings from twenty-nine ESRD patients undergoing HD were processed. T waves in 2-min windows were extracted at each hour during an HD session as well as at 48 h after HD start. T wave nonlinear dynamics were characterized by two indices related to the maximum Lyapunov exponent (λ^t, λ^{wt}) and a divergence-related index (η). Morphological variability in the T wave was evaluated by three time warping-based indices (d_w, reflecting morphological variability in the time domain, and d_a and d_a^{NL}, in the amplitude domain). $[K^+]$ was measured from blood samples extracted during and after HD. Stage-specific and patient-specific $[K^+]$ estimators were built based on the quantified indices and leave-one-out cross-validation was performed separately for each of the estimators.
Results: The analyzed indices showed high inter-individual variability in their relationship with $[K^+]$. Nevertheless, all of them had higher values at the HD start and 48 h after it, corresponding to the highest $[K^+]$. The indices η and d_w were the most strongly correlated with $[K^+]$ (median Pearson correlation coefficient of 0.78 and 0.83, respectively) and were used in univariable and multivariable linear $[K^+]$ estimators. Agreement between actual and estimated $[K^+]$ was confirmed, with averaged errors over patients and time points being 0.000 ± 0.875 mM and 0.046 ± 0.690 mM for stage-specific and patient-specific multivariable $[K^+]$ estimators, respectively.
Conclusion: ECG descriptors of T wave nonlinear dynamics and morphological variability allow noninvasive monitoring of $[K^+]$ in ESRD patients.
Significance: ECG markers have the potential to be used for hypo- and hyperkalemia screening in ESRD patients.

1. Introduction

Chronic kidney disease (CKD) affects 10% of the worldwide population and is associated with increased mortality, decreased quality of life and high economic cost [1]. In the final stage of CKD, so called end-stage renal disease (ESRD), patients can no longer maintain normal serum potassium levels ($[K^+]$). Abnormal $[K^+]$ can cause fatal cardiac arrhythmia [2–5]. Indeed, cardiovascular diseases are the main cause of death in ESRD patients [6] and ventricular arrhythmias are their most common cardiac complication [7]. Changes in $[K^+]$ affect cardiac electrical activity and are reflected in the electrocardiogram (ECG) [2,3, 8–11]. Because of its noninvasive nature and ease of use, markers

---

derived from the ECG are useful tools for $[K^+]$ monitoring and, thus, for risk assessment and triggering early-warning alerts.

The QT interval of the ECG has commonly been used to assess cardiac effects in patients undergoing hemodialysis (HD) [12–17]. However, contradictory findings have been presented in the literature, with some studies reporting QT prolongation with decreasing $[K^+]$ [14,15,17–19] and others reporting QT shortening or no effect [20–22].

Other studies have proposed ECG-derived $[K^+]$ estimators based on the ratio of the T wave slope to the square root of the amplitude [23] and of the T wave slope to the amplitude [24–26]. Additionally, the relationship between $[K^+]$ and the T wave of the ECG has been quantified using characteristics like the trailing slope, amplitude or center of gravity of the T wave and the ratio of the T and R wave amplitudes [27].

ECG markers relying on a specific interval duration or on an amplitude calculated at a single time point may present large variability independent of $[K^+]$ variations, which may be due to noise or wave delineation errors, particularly for low-amplitude waves. In recently published studies [28–30], we proposed the use of warping-based T wave morphology markers to improve estimation of $[K^+]$ changes during HD in ESRD patients. Here, we propose to characterize nonlinear dynamics of the T wave using markers based on maximum Lyapunov exponents and a divergence-related marker. We hypothesized that elevated $[K^+]$ at the start of HD and 48 h later is associated with higher variability in the form of dynamical instabilities, which will be reflected in larger values of the quantified nonlinear dynamics markers [31,32]. In particular, larger repolarization variability at elevated $[K^+]$ would be expected to lead to larger rates of divergence of phase space trajectories associated with T waves and, consequently, higher Lyapunov exponents. This type of $[K^+]$-related changes in nonlinear dynamics could be complementary to other types of T wave morphology, duration and amplitude changes investigated previously. Next, in our study we evaluated the degree of correlation between each of the analyzed markers and $[K^+]$ in ESRD patients during and after HD. Univariable and multivariable regression models including markers of T wave nonlinear dynamics in combination with warping-based markers of T wave morphology were built and their performance for $[K^+]$ estimation was assessed.

2. Methods

2.1. Clinical measurements

48-h 12-lead ECGs, with 3.75 μV resolution and 1 kHz sampling frequency (H12+, Mortara Instruments, Milwaukee, WI, USA), were collected from 29 ESRD patients undergoing HD at Hospital Clínico Universitario de Zaragoza (HCUZ) (Fig. 1). Concurrently, six blood samples were taken, five during the HD session and one 48 h after HD start, with patients in supine position. The first blood sample was taken at the HD onset (h_0) and the next three samples (h_1, h_2 and h_3), every hour during the HD session (Fig. 1 in red). The fifth sample (h_4) was taken at the end of the session (minute 215 or 245, depending on the patient) and the sixth 48 h after the start, immediately before the next session (h_{48}). $[K^+]$ was measured from the extracted blood samples using

a Cobas 6000 c501 analyzer (Roche Diagnostic, Germany) by an indirect ion selective electrode method. The Research Ethics Committee of Aragón approved the study protocol (*CEICA*, ref. PI18/003) on February 14, 2018, and all patients gave signed informed consent. Table 1 shows demographic population characteristics, $[K^+]$ and $[Ca^{2+}]$ values, as well as HD duration and dialysate composition.

A flow chart from ECG pre-processing to the determination of the estimators is shown in Fig. 2.

2.2. ECG pre-processing

ECG signals were band-pass filtered (0.5–40 Hz) to remove baseline wander, muscular noise and powerline interference. QRS detection and wave delineation were performed in each ECG lead using a wavelet-based delineation method [33]. To highlight the T waves, spatial principal components (PCs) were derived from the T waves of the eight independent leads [29,34] in a stable 10-min ECG segment at the end of the HD session. This segment was selected because it corresponded to the time when the patient was discharged from hospital with restored serum $[K^+]$. The full ECG recording was then projected onto the direction of the first PC and used for further analysis that involves evaluation of different segments along the recording. The onset, peak and end of the T waves were delineated on the projection onto the first PC using the same wavelet-based delineation method [33] and the markers such obtained were used in all subsequent analysis.

2.3. T wave morphology markers

Time-warping methods were used to compute T wave morphological descriptors, as previously described [28,29,35]. Two-minute ECG

Table 1
Characteristics of the ESRD study population. Values are expressed as number (*%*) for categorical variables and median (interquartile range) for continuous variables.

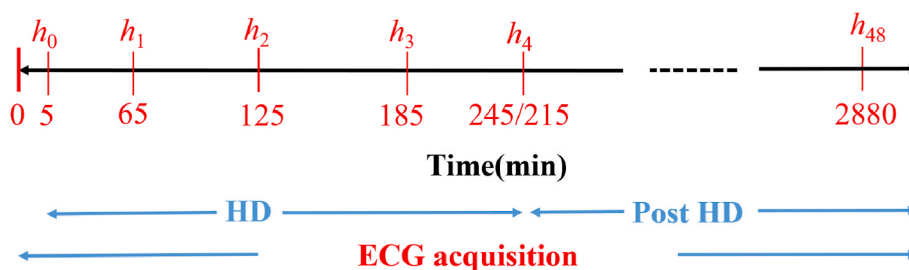| Characteristics	Quantity
Age [years]	75 (12)
Gender [male/female]	20 (69%)/9 (31%)
Electrolyte concentrations	
$[K^+]$ [Pre HD] (mM)	5.05 (1.57)
$[K^+]$ [End HD] (mM)	3.35 (0.62)
$[Ca^{2+}]$ [Pre HD] (mM)	2.15 (0.18)
$[Ca^{2+}]$ [End HD] (mM)	2.32 (0.20)
	#Patients (%)
HD session duration	
240 min	26 (90%)
210 min	3 (10%)
Dialysate composition	
Potassium (1.5 mM)	21 (73%)
Potassium (3 mM)	5 (17%)
Potassium (variable mM)	3 (10%)
Calcium (0.75 mM)	8 (28%)
Calcium (0.63 mM)	21 (72%)

Fig. 1. Diagram of the study protocol. h_0 to h_4 and h_{48} are the time stages corresponding to blood sample extraction, with indication of the time in minutes from the start of the ECG acquisition.
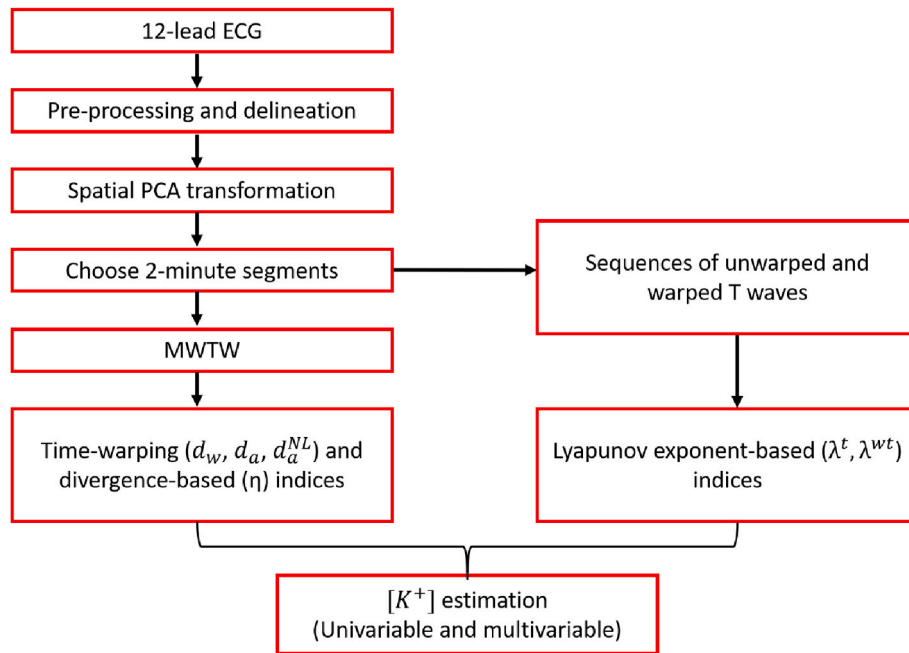
Fig. 2. Flow chart showing the ECG processing steps performed in this study, from the collection of raw ECGs to the estimation of $[K^+]$.

segments at the HD start (h_0), at the end of each HD hour (h_1 to h_4) and at 48 h (h_{48}) were analyzed to compute mean warped T waves (MWTWs), which are optimal representative averages obtained after time-warping all the T waves in the analyzed segment [35]. The predominant T wave polarity was identified as the most frequent polarity in the analyzed 2-min window, with an average of 90% of T waves in each analyzed segment found to present such predominant polarity (see Fig. S1 in Supplementary Material) [28,29]. For MWTW computation, only the T waves having the predominant polarity were considered after alignment with respect to their gravity center [35] so that the calculated MWTW was not affected by potential outlier T waves. This procedure provided an initial MWTW. Next, the subset of T waves presenting wave durations within reported limits and a Spearman correlation coefficient > 0.98 with the computed initial MWTW was selected and the final MWTW for the segment was obtained [28,29]. For each patient, a reference T wave was defined as the MWTW computed at the end of the HD session (h_4).

The MWTW for a given segment was denoted as $\mathbf{f}^s(\mathbf{t}^s) = [f^s(t^s(1)), \ldots, f^s(t^s(N_s))]^\top$ and the reference T wave as $\mathbf{f}^r(\mathbf{t}^r) = [f^r(t^r(1)), \ldots, f^r(t^r(N_r))]^\top$, where $\mathbf{t}^r = [t^r(1), \ldots, t^r(N_r)]^\top$, $\mathbf{t}^s = [t^s(1), \ldots, t^s(N_s)]^\top$ and N_r and N_s are the total durations of $\mathbf{t}^r$ and $\mathbf{t}^s$. Let $\gamma(\mathbf{t}^r)$ be the warping function that relates $\mathbf{t}^r$ and $\mathbf{t}^s$, such that $\mathbf{f}^s(\gamma(\mathbf{t}^r))$ denotes the reparametrization of $\mathbf{f}^s(\mathbf{t}^s)$ using $\gamma(\mathbf{t}^r)$. The square-root slope function (SRSF) transformation was used to find the optimal warping function, $\gamma^*(\mathbf{t}^r)$, defined as the function γ minimizing the amplitude difference between the SRSF of the $\mathbf{f}^s(\gamma(\mathbf{t}^r))$ and $\mathbf{f}^r(\mathbf{t}^r)$ waves [35].

Fig. 3(a) shows $\mathbf{f}^r$ (blue) and $\mathbf{f}^s$ (red), with their respective time domains, $\mathbf{t}^r$ and $\mathbf{t}^s$. The optimally warped T wave (red), $\mathbf{f}^s(\gamma^*(\mathbf{t}^r))$, is shown in Fig. 3(b), together with the reference T wave (blue), $\mathbf{f}^r(\mathbf{t}^r)$. The inter-MWTW difference $\mathbf{f}^d(\mathbf{t}^r)$, shown in black in Fig. 3(b), was computed as the difference between the MWTW $\mathbf{f}^s(\gamma^*(\mathbf{t}^r))$ and the reference $\mathbf{f}^r(\mathbf{t}^r)$:

$$\mathbf{f}^d(\mathbf{t}^r) = \mathbf{f}^s(\gamma^*(\mathbf{t}^r)) - \mathbf{f}^r(\mathbf{t}^r). \tag{1}$$

The time-warping marker d_w, computed as in Refs. [29,35] and shown as the green area in Fig. 3 (d), quantified the level of warping required to optimally align the T waves $\mathbf{f}^s(\mathbf{t}^s)$ and $\mathbf{f}^r(\mathbf{t}^r)$.

The amplitude marker d_a, computed as the area contained between $\mathbf{f}^r(\mathbf{t}^r)$ and $\mathbf{f}^s(\gamma^*(\mathbf{t}^r))$ normalized by the L^2-norm of $\mathbf{f}^r(\mathbf{t}^r)$, quantified the amplitude differences after time warping the two T waves [35].

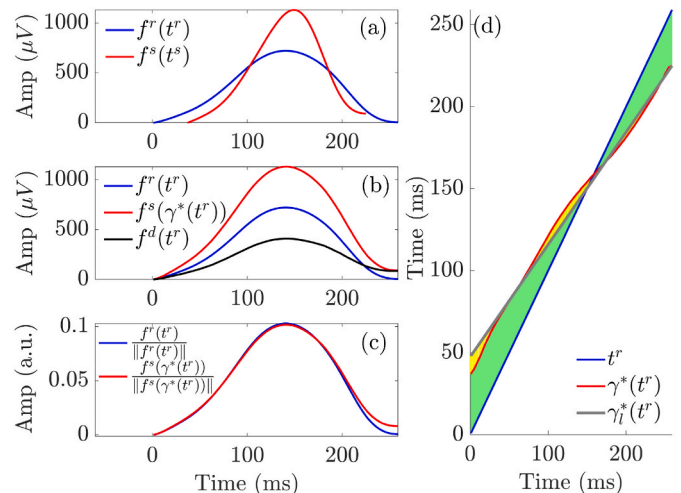The marker d_w incorporates information from the linear and

Fig. 3. Time-warping analysis for one ECG recording. Panel (a) shows reference (blue) and investigated (red) T waves obtained from an ECG segment during HD. Panel (b) shows the warped T waves, which have the same duration while keeping the original amplitude, and the difference between them (black). Panel (c) shows the warped T waves after normalization by their L-2 norms. In panel (d), the green area between the blue line and the red curve represents d_w, which quantifies the total amount of warping in the time domain. The dark gray solid line is the linear regression function $\gamma_l^*(t^r)$ best fitted to $\gamma^*(t^r)$.

nonlinear warping required to match both T waves in the time domain. Similarly, the marker d_a incorporates information in the amplitude domain. The nonlinear components of d_a, denoted by d_a^{NL}, were additionally quantified as described in Refs. [28,29,35].

The warping-based T wave markers during (h_0, h_1, h_2, h_3, h_4) and after (h_{48}) HD included:

- d_w, representing temporal variations in T wave morphology (expressed in ms),
- d_a, representing amplitude variations in T wave morphology (expressed as %), and

- d_a^{NL}, representing nonlinear amplitude variations in T wave morphology (expressed as %).

2.4. T wave nonlinear dynamics markers

T wave nonlinear dynamics were characterized by computing markers based on maximum Lyapunov exponents computed using Rosenstein's method [36] and another divergence-related marker, as follows.

2.4.1. Lyapunov exponent-based markers λ^t and λ^{wt}

Let's consider 2-min ECG segments as defined above for each analyzed patient and HD stage. The sequence of concatenated T waves for each of these segments, after having tilted the waves to make their onset and end have zero amplitude, is denoted by:

$$\mathbf{f} = [\mathbf{f}_1^\top, \mathbf{f}_2^\top, ..., \mathbf{f}_B^\top]^\top = [f(1), f(2), ..., f(N)]^\top \qquad (2)$$

with $\mathbf{f}_k = [f_k(1), f_k(2), ..., f_k(N_k)]^\top$ denoting the k-th T wave of N_k samples (i.e. of duration N_k ms, since the sampling frequency is 1 kHz), B the number of beats in the segment and $N = \sum_{k=1}^{B} N_k$ the number of samples of sequence $\mathbf{f}$. Fig. 4, panels (a)–(c), shows T waves in three analyzed segments of an ECG recording.

The reconstructed trajectories for delay values of τ were represented by vectors

$$\mathbf{f}^{(\tau)}(j) = [f(j), f(j+\tau), ..., f(j+(m-1)\tau)]^\top \qquad (3)$$

with $j \in \{1, 2, ..., M\}$ and $M = N - (m-1)\tau$, where m is the embedding dimension, here set to 30, and τ the delay in ms, here set to $\lceil N_1/(m-1) \rceil$, where N_1 is the duration of the first T wave, in ms. For each $\mathbf{f}^{(\tau)}(j)$, its nearest neighbor $\mathbf{f}^{(\tau)}(\hat{j})$ was searched for by minimizing

$$d_j(0) = \min_{\mathbf{f}^{(\tau)}(\hat{j})} ||\mathbf{f}^{(\tau)}(j) - \mathbf{f}^{(\tau)}(\hat{j})||, \qquad (4)$$

with $|j - \hat{j}| > p$, and p set to 25. The notation $|| \cdot ||$ represents the L2 norm.

Next, the distance between the nearest neighbors $\mathbf{f}^{(\tau)}(j)$ and $\mathbf{f}^{(\tau)}(\hat{j})$ was computed after i steps as:

$$d_j(i) = ||\mathbf{f}^{(\tau)}(j+i) - \mathbf{f}^{(\tau)}(\hat{j}+i)||, \qquad (5)$$

where $i = 1, 2, ..., I$, and $I = \lceil N/5 \rceil$.

For each value of i, the average $y(i)$ of the logarithm of the functions $d_j(i)$ for $j = 1, 2, ..., M - I$, was computed as:
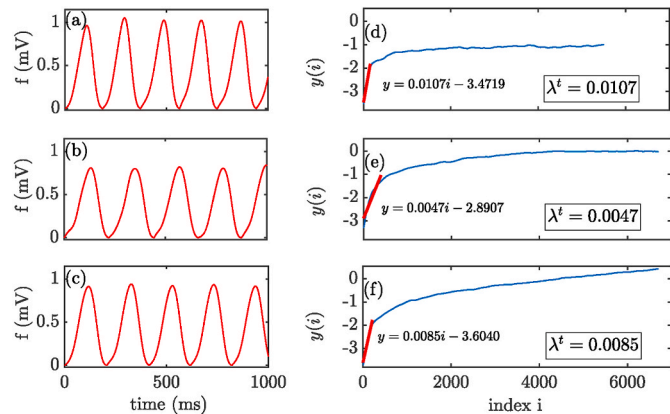
$$y(i) = \frac{1}{M-I} \sum_{j=1}^{M-I} \ln(d_j(i)). \qquad (6)$$

The largest Lyapunov exponent λ^t was estimated as the slope of the least-squares fit to the initial linear portion of $y(i)$, $i = 1, ..., c_p$, with c_p being the point where the signal changes most rapidly in mean and slope [37]. Despite being computed from the linear portion of $y(i)$, this index accounts for nonlinear dynamics of the T wave, as can be observed from equations (2)–(6).

Fig. 4, panels (d)–(f), shows λ^t from a patient at three different HD stages (h_0, h_1, h_{48}) and the corresponding functions $y(i)$ for varying i together with its linear fit for $i = 1, ..., c_p$.

Additionally, another marker, denoted by λ^{wt}, was estimated from the same sequence of T waves in the analyzed 2-min segments but after warping. The procedure used to calculate λ^{wt} was the same as above but with $\mathbf{f}$ representing the sequence of concatenated warped T waves in the 2-min segment. The calculation of λ^{wt} and its comparison with λ^t serves to analyze the contribution of amplitude variability, separately from time variability, to the maximum Lyapunov exponent.

2.4.2. Divergence-related marker η

T wave nonlinear dynamics were further evaluated by computing the marker η based on the divergence of trajectories from the inter-MWTW difference defined in equation (1). Specifically, η was computed by averaging $y_d(i)$ from $i = c_p + 1$ to $i = I$:

$$\eta = \frac{1}{I - c_p} \sum_{i=c_p+1}^{I} y_d(i), \qquad (7)$$

where $y_d(i)$ was computed as $y(i)$ in (6) but for the inter-MWTW $\mathbf{f}^d$ rather than for $\mathbf{f}$. In the calculation of $y_d(i)$, $M = N - (m-1)\tau$, where $m = 22$, $\tau = 3$ ms and $p = 25$, with N the duration of the inter-MWTW $\mathbf{f}^d$ in ms.

Fig. 5 shows η for inter-MWTW $\mathbf{f}^d$ from a patient at different HD stages (h_0, h_1, h_{48}) as well as the corresponding functions $y_d(i)$ for varying i. Values of η for T waves from different ECG segments with distinct wave morphologies (upright, inverted, biphasic) and their functions $y_d(i)$ for varying i are shown in the Supplementary Material (Fig. S2).

For calculation of η, inter-MWTW at h_4 was computed by taking the difference between the reference T wave and a MWTW computed from the 2-min ECG segment just before the segment taken at the end of the HD hour.

2.5. Synthetically generated T waves

The ability of λ^t, λ^{wt}, η, d_w, d_a and d_a^{NL} to capture gradual linear and nonlinear T wave time and amplitude variations along time, both in the

Fig. 4. Panels a–c: A few T waves from 2-min ECG segments for a particular patient at different HD stages (h_0, h_1, h_{48}). Panels d–f: $y(i)$ versus index i varying from 1 to I as described in the text. Values of λ^t obtained as the slope of $y(i)$ are shown for each HD time point.
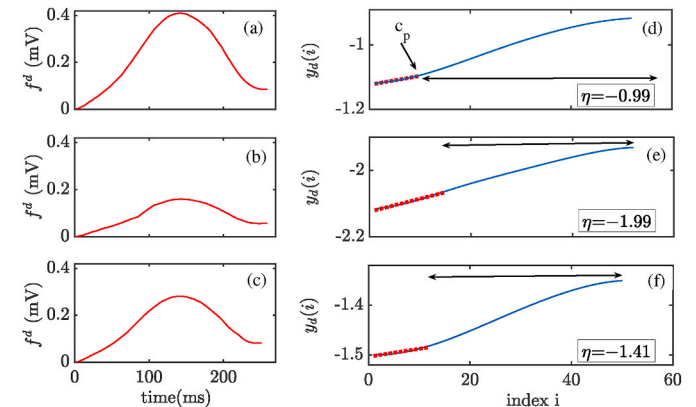

Fig. 5. Panels a–c: Inter-MWTWs from a particular patient at different HD stages (h_0, h_1, h_{48}). Panels d–f: $y_d(i)$ computed as described in the text, with indication of the corresponding η values.

absence and presence of temporal inter-beat variability, was assessed by generating sets of synthetic T waves in which changes were simulated according to specifically defined functions, as described in the following.

2.5.1. Simulation of T wave duration and amplitude changes

We considered a preprocessed PCA-transformed T wave obtained from a particular patient as a reference T wave, $\mathbf{f}^r(\mathbf{t}^r)$. We defined nonlinear T wave amplitude changes by:

$$\mathbf{f}^k_{\mathrm{NL}}(\mathbf{t}^r) = \mathbf{f}^r(\mathbf{t}^r) + c(k)\sin\left(2\pi\frac{1}{4N_r}\mathbf{t}^r\right), \tag{8}$$

where $c(k) = 25\sin[\pi(B_{\mathrm{T}}+k)/(2B_{\mathrm{T}})]$ being $k = 1, \ldots, B_{\mathrm{T}}$ the index of a T wave and B_{T} the total number of simulated beats, which was set to the number of beats during the whole HD session in the patient from whom the reference T wave was selected. The simulated T waves in the first 2-min segment were identified as representative of h_0, while the simulated T waves for beats in 2-min segments at the end of the first, second, third and fourth hours were taken as representative of h_1, h_2, h_3 and h_4, respectively.

Additional linear T wave amplitude changes were generated on top of the nonlinear amplitude changes:

$$\mathbf{f}^k_l(\mathbf{t}^r) = \mathbf{f}^k_{\mathrm{NL}}(\mathbf{t}^r)\cdot b(k) \tag{9}$$

where $b(k) = 1 + 0.25\sin(\pi(B_{\mathrm{T}} + k)/(2B_{\mathrm{T}}))$.

Nonlinear T wave duration changes were generated as follows:

$$\mathbf{t}^k_{\mathrm{NL}} = \mathbf{t}^r + g(k)\frac{N_r}{N_k}\cdot\sin\left(2\pi\frac{1}{N_r}\mathbf{t}^r\right), \tag{10}$$

where $g(k) = 10\frac{k-1}{B_{\mathrm{T}}-1} - 10$.

Additional linear T wave duration changes were simulated on top of the nonlinear duration changes:

$$\mathbf{t}^k_l = \gamma_k(\mathbf{t}^k_{\mathrm{NL}}), \tag{11}$$

where $\gamma_k(\mathbf{t}^k_{\mathrm{NL}})$ stretches $\mathbf{t}^k_{\mathrm{NL}}$ according to a downsampling factor $a(k) = 0.25\frac{k-1}{B_{\mathrm{T}}-1} + 0.75$.

Combined simulated T wave duration and amplitude changes were defined according to:

$$\mathbf{f}^k_{\mathrm{S}}(\mathbf{t}^k) = \mathbf{f}^k_l(\mathbf{t}^k_l). \tag{12}$$

In this study, we used six different cases, $C\#$, which corresponded to linear and nonlinear duration and amplitude changes in the T waves:

- $C1$ considered the reference T wave and maintained its duration and amplitude along the whole simulation
- $C2$, defined by nonlinear amplitude changes,
- $C3$, defined by linear amplitude changes on top of nonlinear amplitude ones,
- $C4$, defined by nonlinear duration changes,
- $C5$, defined by linear duration changes on top of nonlinear duration ones, and
- $C6$, corresponding to the combined effects of linear and nonlinear amplitude and duration modulations in the T waves.

2.5.2. Simulation of temporal inter-beat variability

Realistic variability signals were obtained from an ESRD patient, with index q_0, for each 2-min segment representative of each stage during and after HD. Variability signals were defined as the difference of each individual aligned T wave and the corresponding average in the 2-min window:

$$\mathbf{f}^k_v = \mathbf{f}^k_{v,q_0} = \mathbf{f}^k - \frac{1}{B}\sum_{k=1}^{B}\mathbf{f}^k. \tag{13}$$

To make the magnitude of temporal inter-beat variability be representative of the averaged variability over patients rather than representative of an individual patient, the following factors were computed for each patient in a 2-min window around each HD stage point and the median over all patients was calculated. Two different approaches were used to compute the factors associated with variability modulation in each patient. On the one hand, inter-beat variability factors at a given HD stage were defined for each patient q as:

$$\alpha^{\mathrm{Inter}}_{v,q} = \frac{1}{N^{\mathrm{Inter}}}\sum_{n=1}^{N^{\mathrm{Inter}}} f^{\mathrm{Inter}}_{\mathrm{IQR}_{v,q}}(n), \tag{14}$$

$$f^{\mathrm{Inter}}_{\mathrm{IQR}_{v,q}}(n) = \mathrm{IQR}\{f^1_{v,q}(n), f^2_{v,q}(n), \ldots, f^B_{v,q}(n)\}, \tag{15}$$

where IQR represents the interquartile range operation, B is the number of beats in the 2-min segment and N^{Inter} is the number of samples in the $\mathbf{f}^{\mathrm{Inter}}_{\mathrm{IQR}_v}$.

Similarly, intra-beat variability factors at a given HD stage were defined for each patient q as:

$$\alpha^{\mathrm{Intra}}_{v,q} = \frac{1}{B}\sum_{k=1}^{B} f^k_{\mathrm{IQR}_{v,q}}, \tag{16}$$

$$f^k_{\mathrm{IQR}_{v,q}} = \mathrm{IQR}\{f^k_{v,q}(1), f^k_{v,q}(2), \ldots, f^k_{v,q}(N_k)\}. \tag{17}$$

Representative scaling factors accounting for information from all patients, denoted by $\widetilde{\alpha}^{\mathrm{Inter}}_v$ and $\widetilde{\alpha}^{\mathrm{Intra}}_v$, were calculated by taking the median of the variability factors $\alpha^{\mathrm{Inter}}_{v,q}$ and $\alpha^{\mathrm{Intra}}_{v,q}$ over all patients. The calculated factors were applied to the variability signal, $\mathbf{f}^k_v$, and added to the synthetic T wave, $\mathbf{f}^k_{\mathrm{S}}$, obtained as described in section 2.5.1, to have representative variability in the simulation:

$$\mathbf{f}^k_{\mathrm{S}+v_{\mathrm{Inter}}} = \frac{\widetilde{\alpha}^{\mathrm{Inter}}_v}{\alpha^{\mathrm{Inter}}_{v,q_0}}\cdot\mathbf{f}^k_{v,q_0} + \mathbf{f}^k_{\mathrm{S}}, \tag{18}$$

and

$$\mathbf{f}^k_{\mathrm{S}+v_{\mathrm{Intra}}} = \frac{\widetilde{\alpha}^{\mathrm{Intra}}_v}{\alpha^{\mathrm{Intra}}_{v,q_0}}\cdot\mathbf{f}^k_{v,q_0} + \mathbf{f}^k_{\mathrm{S}}, \tag{19}$$

where $\alpha^{\mathrm{Inter}}_{v,q_0}$ and $\alpha^{\mathrm{Intra}}_{v,q_0}$ were computed from the variability signals of the particular patient q_0.

For each analyzed HD stage, the generated T waves with added variability, i.e. $\mathbf{f}^k_{\mathrm{S}+v_{\mathrm{Inter}}}$ and $\mathbf{f}^k_{\mathrm{S}+v_{\mathrm{Intra}}}$, were concatenated for all simulated beats $k = 1, 2, \ldots, B$.

Additionally, MWTWs and inter-MWTWs were computed from simulated T waves in 2-min segments to assess the response of d_w, d_a, d_a^{NL} and η to the simulated duration and amplitude changes, both with and without additional scaled intra-beat variability. Inter-beat variability was used to assess the performance of λ^t and λ^{wt}.

2.6. Correlation analysis and statistical comparisons

To assess the relationship between each investigated T wave marker and $[\mathrm{K}^+]$ during and after HD, Pearson and Spearman correlation analyses were performed for each patient.

To quantify the relationship of T wave markers and $[\mathrm{K}^+]$ independently of other factors known to affect the T wave like serum calcium concentration ($[\mathrm{Ca}^{2+}]$) or the RR interval, linear partial correlation analysis was performed for each patient.

The duration of the ECG recordings was 48 h for all patients, except for a few that ended some minutes earlier, mainly due to electrode detachment or battery exhaustion. However, given the small expected drift of $[\mathrm{K}^+]$ in this short time period, we assumed that the end of the ECG recording corresponded to the $[\mathrm{K}^+]$ blood sample taken at 48 h. For this reason, correlation coefficients were computed using the five values of $[\mathrm{K}^+]$ at HD stages h_i, $i \in \{0, 1, 2, 3, 4\}$, as well as at $i = 48$ h.

Wilcoxon signed-rank tests were performed to test for significant differences in λ^t, λ^{wt}, η, d_w, d_a and d_a^{NL} at different time stages during and after HD. The use of a nonparametric statistical test was based on the lack of normality of the data distributions according to Shapiro-Wilk test. $p < 0.05$ was considered statistically significant.

Student's t-test was applied to test whether Pearson correlation coefficient r between each T wave marker and $[K^+]$ was significantly different from 0 in mean over the population, after converting the statistical distribution of r into a normal distribution using Fisher's z transform [38].

The performance of our investigated T wave markers was compared with that of the previously proposed T wave markers $T_{S/A}$ [25,26] and $T_{S/\sqrt{A}}$ [23], which were computed from MWTWs at time points h_0, h_1, h_2, h_3, h_4 and h_{48} during and after HD (see Supplementary Material):

- $T_{S/A}$, representing the ratio between the maximal downward slope (in absolute value) and the amplitude of the T wave [25,26].
- $T_{S/\sqrt{A}}$, representing the ratio between the maximal downward slope (in absolute value) and the square root of the amplitude of the T wave [23].

All statistical analyses were performed using MATLAB version R2020a for Windows (MathWorks Inc., MI, USA).

2.7. Univariable and multivariable estimation of $[K^+]$

To estimate $[K^+]$ from the analyzed T wave markers, univariable and multivariable linear regression models were built. The univariable models included either η or d_w and the multivariable model included both.

The univariable estimators $[K^+]^{d_w}$ and $[K^+]^{\eta}$ and the multivariable estimator $[K^+]^m$ were defined as:

$$[K^+]^{\eta} = \beta_0^{\eta} + \beta_1^{\eta} \cdot \eta, \tag{20}$$

$$[K^+]^{d_w} = \beta_0^{d_w} + \beta_1^{d_w} \cdot d_w, \tag{21}$$

$$[K^+]^m = \beta_0^m + \beta_1^m \cdot \eta + \beta_2^m \cdot d_w. \tag{22}$$

For the univariable models, the coefficients $\boldsymbol{\beta} = \begin{bmatrix} \beta_0^{\eta} & \beta_1^{\eta} \end{bmatrix}^T$ or $\boldsymbol{\beta} = \begin{bmatrix} \beta_0^{d_w} & \beta_1^{d_w} \end{bmatrix}^T$ were computed as:

$$\widehat{\boldsymbol{\beta}} = (\mathbf{X}^T \mathbf{X})^{-1} \mathbf{X}^T \mathbf{y}^T, \tag{23}$$

with $\mathbf{X} = \begin{bmatrix} \mathbf{j}^T & \mathbf{x}_b^T \end{bmatrix}$. The definition of $\mathbf{j}^T$, $\mathbf{x}_b^T$ and $\mathbf{y}$ is different for time- and patient-specific estimators, as described in the following.

For a given HD stage i, the stage-specific estimator $\widehat{\boldsymbol{\beta}}$ was calculated from equation (23) by considering $\mathbf{j} = [1, 1, ..., 1]$ of dimension $1 \times Q$, with Q the number of patients. The vector $\mathbf{x}_b = [b_{i,1}, b_{i,2}, ..., b_{i,Q}]$ contained the values of the marker b, being either η or d_w at the considered HD stage i from all the patients $q = 1, ..., Q$. The vector $\mathbf{y} = [[K^+]_{i,1}, [K^+]_{i,2}, ..., [K^+]_{i,Q}]$, contained the measured values of $[K^+]$ at the HD stage i for all patients.

For a given patient q, the patient-specific estimator $\widehat{\boldsymbol{\beta}}$ was calculated by considering $\mathbf{j} = [1, 1, ..., 1]$ of dimension 1×6. The vector $\mathbf{x}_b = [b_{0,q}, b_{1,q}, b_{2,q}, b_{3,q}, b_{4,q}, b_{48,q}]$ contained the values of b, either η or d_w, for patient q at all HD stages $i = 0, 1, 2, 3, 4, 48$. The vector $\mathbf{y} = [[K^+]_{0,q}, [K^+]_{1,q}, [K^+]_{2,q}, [K^+]_{3,q}, [K^+]_{4,q}, [K^+]_{48,q}]$ contained the measured values of $[K^+]$ values for patient q at all HD stages i.

For the multivariable model, $\boldsymbol{\beta} = [\beta_0^m, \beta_1^m, \beta_2^m]^T$ was calculated from equation (23), now using $\mathbf{X} = [\mathbf{j}^T, \mathbf{x}_{b^{(1)}}^T, \mathbf{x}_{b^{(2)}}^T]$, with $\mathbf{x}_{b^{(1)}}$ containing the values of η and $\mathbf{x}_{b^{(2)}}$ containing the values of d_w and defined as described above for either HD-stage- or patient-specific estimators.

Leave-one-out cross validation was used to assess the performance of

the $[K^+]$ estimators:

- *Stage-specific estimators:* The estimator was trained with $Q - 1$ patients for each HD stage individually and then tested for the Q-th patient. This process was repeated for all HD stages.
- *Patient-specific estimators:* The estimator was trained with five HD stage points for each patient individually and tested for the 6th stage. This process was repeated for all patients.

The error ε between measured and estimated $[K^+]$ values was computed as

$$\varepsilon = [K^+]_a - [K^+]_e, \tag{24}$$

where $[K^+]_a$ is $[K^+]$ measured from blood test and $[K^+]_e$ is the estimated $[K^+]$. The relative error R_v was computed as

$$R_v = \frac{[K^+]_a - [K^+]_e}{[K^+]_{\mathcal{D}}}, \tag{25}$$

where $[K^+]_{\mathcal{D}}$ was defined, for each patient, as the difference between maximum and minimum $[K^+]_a$ values across HD stage. The relative error R_r was computed as

$$R_r = \frac{[K^+]_a - [K^+]_e}{[K^+]_{\mathcal{R}}}, \tag{26}$$

where $[K^+]_{\mathcal{R}}$ was defined as the difference between maximum 75th and minimum 25th percentiles of $[K^+]$ across patients at each HD stage.

To assess the agreement between actual and estimated $[K^+]$ values, Bland-Altman analysis was performed [39]. Figures in the Supplementary Material show the difference vs the mean of actual and estimated $[K^+]$ for all patients at all HD time points.

It should be noted that a $[K^+]$ estimator was not computed at the end of the HD session (h_4) since the morphological T wave marker d_w was zero by definition, as the reference was taken at that time stage.

3. Results

3.1. Robust calculation of T wave nonlinear dynamics markers

Fig. 6 shows λ^t, λ^{wt} and η for variations in the values of the parameters p, τ and m around their default values so as to assess the sensitivity of these markers to their parameters. The individual T waves in a 2-min window from a particular patient at a given HD stage were used for the computation of λ^t and λ^{wt}, whereas the corresponding inter-MWTW was used for the computation of η. Thus, the default values of the parameters p, τ and m were different for λ^t and λ^{wt} than for η, as described in section 2.4. As can be seen from Fig. 6, λ^t and λ^{wt} were more sensitive to τ and m than to p but they tended to be stable around the values $\tau = 6$ and $m = 30$ employed here. The marker η, computed from inter-MWTW, was almost stable around the chosen values $p = 25$, $\tau = 3$ and $m = 22$.

3.2. Simulation of changes in T wave amplitude, duration and temporal inter-beat variability

Fig. 7, top panels, shows T waves under simulated linear and nonlinear duration and amplitude changes. Each panel shows the last T wave ($\mathbf{f}_S^k$) in a simulated 2-min segment representing an HD stage. The bottom panels show the variability signals ($\mathbf{f}_v^k$) added to the T waves. Tall and narrow T waves are observed at h_0, representing the situation at the HD start, with a subsequent amplitude decrease and duration increase along time to represent variations during HD.

Fig. 8 shows the evolution of T wave markers (λ^t, η, d_w, d_a and d_a^{NL}) for simulated linear and nonlinear variations in duration and amplitude ($C2$ to $C6$), with (panels f–j) and without (panels a–e) added variability
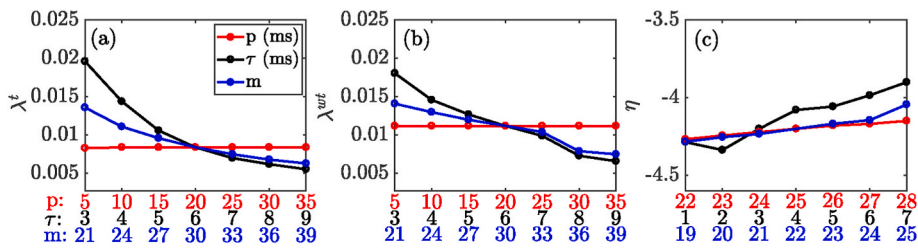
Fig. 6. Panels a–c: Sensitivity of λ^t (left), λ^{wt} (middle) and η (right) for different values of the parameters representing the period (p), delay (τ) and embedding dimension (m) calculated from unwarped and warped T waves in a 2-min window and inter-MWTW of a patient at a particular HD stage (h_4). Note that the default values of p, τ and m used in the calculation of λ^t and λ^{wt} are different from the ones used in the calculation of η, which explains differences in the x-axis of panels (a) and (b) with respect to panel (c).
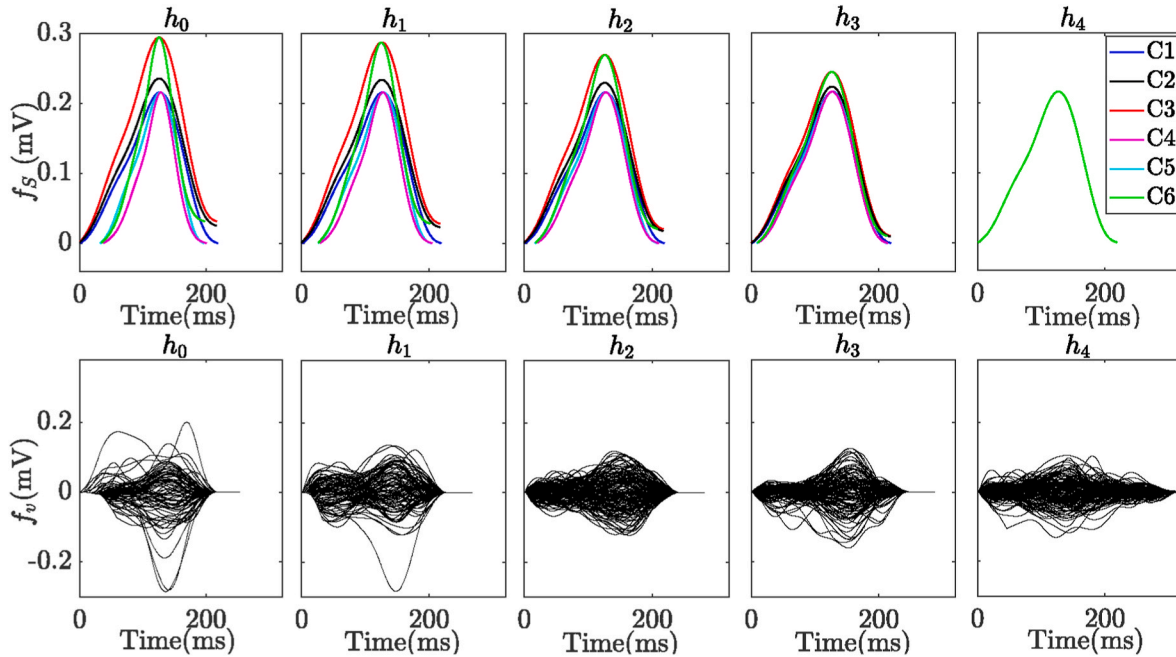

Fig. 7. Simulated (last) T wave from a sequence of 2 min T waves (f_S^k) in linear and nonlinear duration and amplitude domain (top panels) and the variability (f_v^k) in 2 min T waves (bottom panels) during HD. Solid black and red T waves correspond to nonlinear and linear amplitude modulation ($C2$, $C3$), solid cyan and magenta T waves correspond to nonlinear and linear duration modulation ($C4$, $C5$), and solid green T wave includes both time and amplitude modulation ($C6$). Blue T wave corresponds to the reference T wave ($C1$).

to T waves. As can be seen from the figure, the Lyapunov exponent-based marker λ^t reflects temporal inter-beat variability in the T wave well, while the divergence marker η and morphology-based markers d_w, d_a and d_a^{NL} are able to describe linear and nonlinear duration or amplitude changes. The markers d_w and η are the ones best reflecting simulated time changes and combined time and amplitude changes in the T wave, respectively. Results for λ^{wt} were similar to those obtained for λ^t, although the decreasing trend along simulated time was less clear.

3.3. Characterization of T wave changes during and after HD

Fig. 9, panels a–f, shows the changes in the analyzed T wave markers (λ^t, λ^{wt}, η, d_w, d_a and d_a^{NL}) together with [K$^+$] changes during and after the HD session for the analyzed ESRD patients' recordings. Illustrative T waves for a patient are shown in the bottom panels g–h, presenting the reference T wave (blue), each investigated T wave (red) and inter-MWTW (black) during and after the HD session, both before (panel g) and after (panel h) warping and averaging.

A decreasing trend in all markers (right y-axis, in red) with decreasing [K$^+$] (left y-axis, in blue) was observed during HD, from h_0 (HD start) to h_4 (HD end). The marker values increased with increasing [K$^+$] from the HD end to the 48-th hour after the HD start. Particularly remarkable changes can be seen for the morphology marker d_w and for the nonlinear dynamics marker η. Since we took the end of the HD

session (h_4) as reference for computation of d_w, d_a and d_a^{NL}, these markers take zero value at this HD stage. From the bottom panels of Fig. 9, tall and narrow T waves can be observed before (h_0) and 48 h after HD (h_{48}), corresponding to the highest [K$^+$] values.

3.4. Correlation between T wave markers and [K$^+$]

Fig. 10 shows the results of the correlation analysis. The linear correlation coefficients between [K$^+$] and each of the T wave markers are shown in black and the partial linear correlation coefficients after removing the effects of RR and [Ca^{2+}] are shown in red and blue, respectively. The markers d_w, η, d_a^{NL} and λ^t were the most highly linearly correlated with [K$^+$], with median Pearson r over patients presented in Table 2 λ^{wt} and d_a poorly correlated with [K$^+$]. Also, d_w and η were the most strongly correlated with [K$^+$] after removing the effects of RR and these two indices, together with d_a and d_a^{NL}, were the most strongly correlated with [K$^+$] after removing the effects of [Ca^{2+}]. Results obtained for Pearson and Spearman correlation coefficients between [K$^+$] and each the T wave markers investigated in this study and others previously proposed in the literature are presented in Table SI of the Supplementary Material, with the highest values obtained for d_w, η and $T_{S/A}$.

Table 2 also shows the p-values from Student's t-test to assess the statistical significance of non-zero mean Fisher's z-transformed Pearson
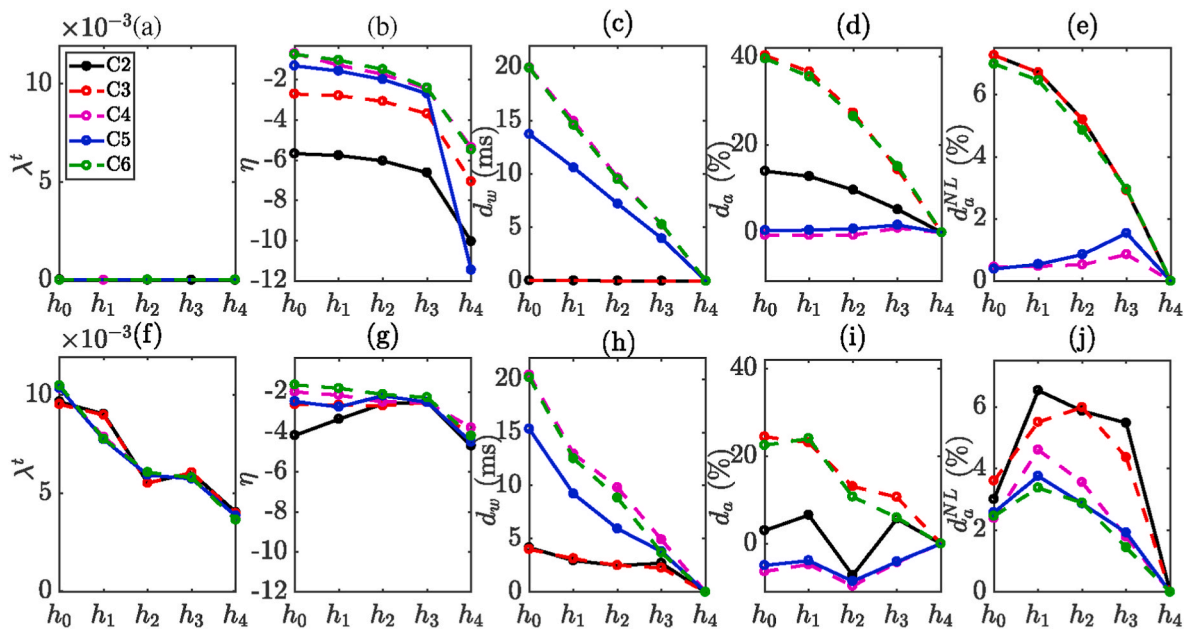
Fig. 8. Panels a–j: T wave markers (λ, η, d_w, d_a and d_a^{NL}) in linear and nonlinear duration and amplitude simulations during HD, with (bottom panels f–j) and without (top panels a–e) adding scaled variability's. Solid black and dotted red results correspond to nonlinear and combined nonlinear and linear amplitude modulation ($C2$, $C3$), dotted cyan and solid blue results correspond to nonlinear and combined nonlinear and linear duration modulation ($C4$, $C5$), and dotted green results includes both time and amplitude modulations ($C6$).
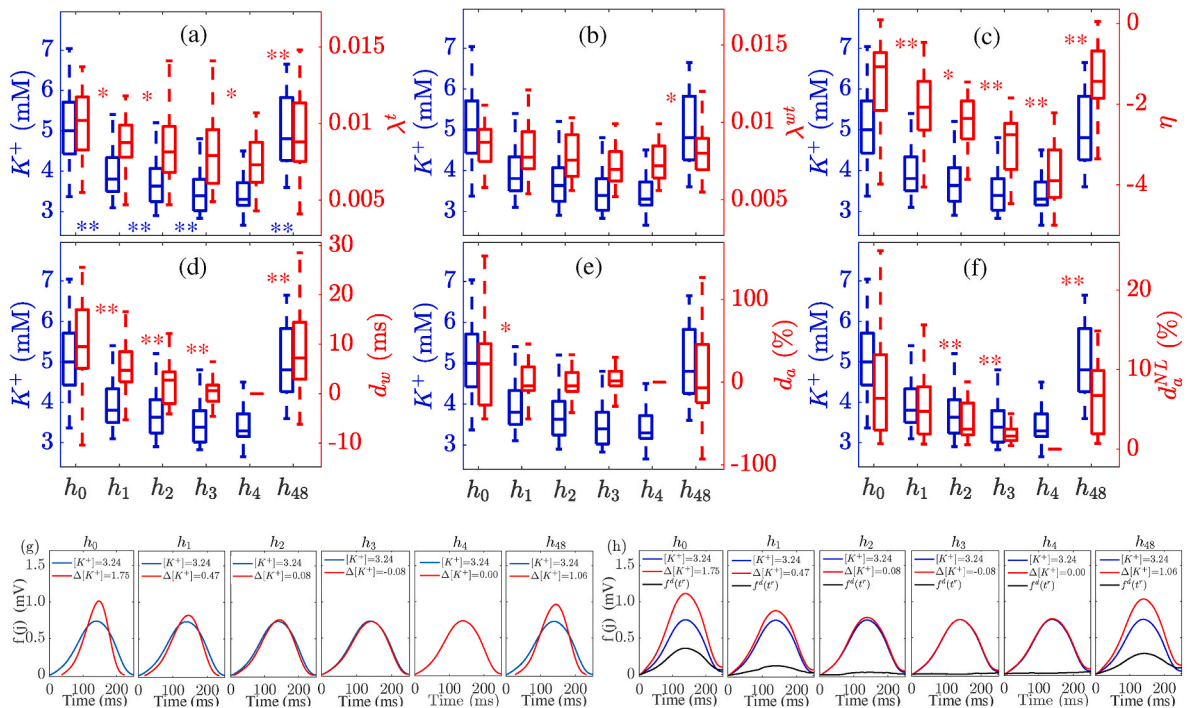

Fig. 9. Panels a–f: Changes in λ^t, λ^{wt}, η, d_w, d_a and d_a^{NL} with [K^+] variations for the analyzed patients' recordings during and after HD. In panels a–f, * indicates $p < 0.05$ and ** indicates $p < 0.01$ in the comparison of each marker between consecutive time stages. The central line indicates the median, whereas top and bottom edges show the 25th and 75th percentiles, respectively. Panel g: T waves of a patient during and after HD. Panel h: Warped T waves of a patient during and after HD, with the reference T wave (blue), each analyzed T wave (red) and inter-MWTW (black) being displayed. Δ denotes the change in [K^+] with respect to the end of the HD session and the units in the legends of panels (g) and (h) are mM.

correlation coefficients between T wave markers and [K^+]. As can be seen from the table, all the analyzed T wave markers, except for d_a and λ^{wt}, correlated significantly with [K^+].

To confirm that T wave nonlinear dynamics markers (λ^t, λ^{wt} and η) provided complementary information to morphological markers (d_w, d_a

and d_a^{NL}), linear correlation analysis was performed and results are shown in Table 3. As can be observed, the markers d_a^{NL} and η correlated strongly.
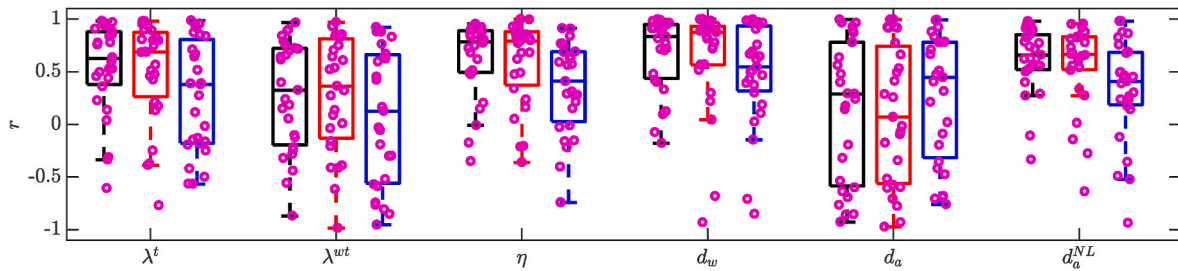
Fig. 10. Correlation coefficients between T wave markers (λ^t, λ^{wt}, η, d_w, d_a, and d_a^{NL}) and [K$^+$] from patients' ECGs. Black boxplots: Pearson correlation coefficients. Red boxplots: Partial linear correlation coefficients after removing the effects of RR. Blue boxplots: Partial linear correlation coefficients after removing the effects of [Ca^{2+}]. Each purple dot represents the correlation coefficient for an individual patient. The central line indicates the median, whereas top and bottom edges show the 25th and 75th percentiles, respectively.

Table 2

Median pearson r and partial correlation coefficients after removing the effects of RR (r_{RR}) and [Ca^{2+}] ($r_{[Ca^{2+}]}$), and P-values from student's T-test to evaluate statistical significance of non-zero mean fisher's Z-transformed pearson correlation coefficient between T wave markers and [K$^+$].

[K$^+$]	λ^t	λ^{wt}	η	d_w	d_a	d_a^{NL}
r	0.63	0.32	0.78	0.83	0.29	0.66
r_{RR}	0.69	0.36	0.79	0.87	0.07	0.66
$r_{[Ca^{2+}]}$	0.38	0.12	0.41	0.54	0.45	0.41
p-values	<0.01	0.01	<0.01	<0.01	0.18	<0.01

Table 3

Intra-patient pearson correlation coefficients (r) between morphological and nonlinear dynamics T wave markers.

Parameter	λ^t	λ^{wt}	η
d_w	0.66 (0.43)	0.42 (0.58)	0.55 (0.73)
d_a	0.29 (1.25)	0.05 (0.95)	−0.12 (1.62)
d_a^{NL}	0.57 (0.42)	0.21 (0.60)	0.72 (0.25)

*Values are expressed as median (IQR).

3.5. ECG-based estimation of [K$^+$]

Fig. 11 shows the error ε for univariable and multivariable [K$^+$] estimators for all ESRD patients at each HD stage using both stage-specific and patient-specific approaches. Particularly for the multivariable estimator, Table 4 shows the estimated $[K^+]_e^m$ values using stage-specific, $[K^+]_e^{m,S}$, and patient-specific, $[K^+]_e^{m,P}$, approaches and compares them

Table 4

Results for the multivariable $[K^+]_e^m$ estimator at each HD stage. $[K^+]_e^{m,S}$: Estimated [K$^+$] using stage-specific approach; $[K^+]_e^{m,P}$: Estimated [K$^+$] using patient-specific approach.

Actual vs Estimated [K$^+$]	h_0	h_1	h_2	h_3	h_{48}
$[K^+]_a$	5.23 ± 1.10	4.05 ± 0.78	3.70 ± 0.58	3.48 ± 0.52	5.01 ± 0.93
$[K^+]_e^{m,S}$	5.20 ± 0.33	4.05 ± 0.20	3.70 ± 0.16	3.46 ± 0.14	5.04 ± 0.31
$[K^+]_e^{m,P}$	4.78 ± 1.45	4.21 ± 0.68	3.82 ± 0.76	3.63 ± 0.73	4.78 ± 1.26

with the measured $[K^+]_a$ values.

Tables 5 and 6 show the relative errors R_v and R_r between actual and estimated [K$^+$] at each HD stage for the multivariable estimator using stage-specific and patient-specific approaches.

Table 7 shows the median and IQR values of intra-patient Pearson

Table 5

Relative errors R_v using stage-specific (S) and patient-specific (P) approaches for the multivariable estimator.

R_v	h_0	h_1	h_2	h_3	h_{48}
S	−0.20 ± 0.68	−0.13 ± 0.45	−0.10 ± 0.35	−0.07 ± 0.29	−0.17 ± 0.57
P	0.30 ± 0.61	−0.11 ± 0.28	−0.09 ± 0.26	−0.09 ± 0.20	0.18 ± 0.38

*Values are expressed as mean ± standard deviation.

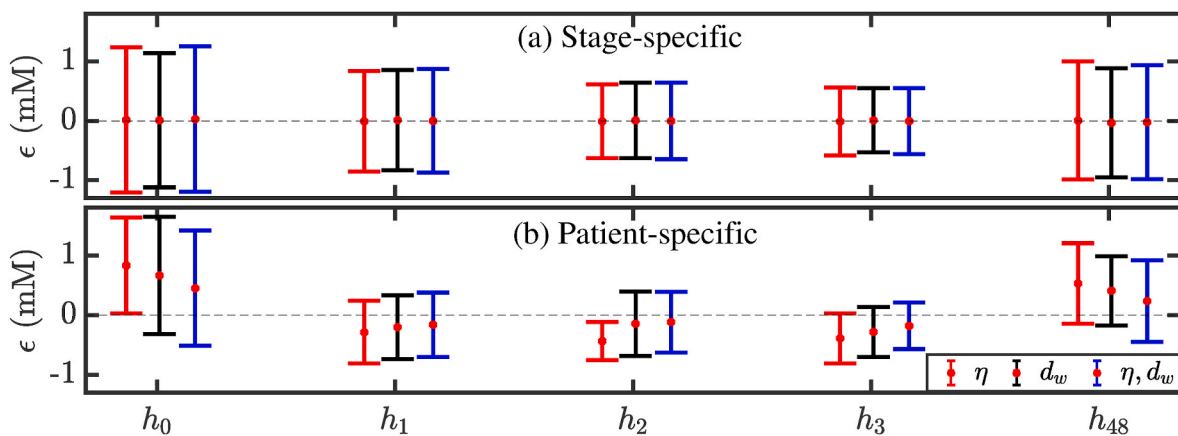**Fig. 11.** Error ε between estimated and actual [K$^+$] for all ESRD patients during and after HD using univariable (η or d_w) and multivariable (η and d_w) estimators with stage-specific (panel (a)) or patient-specific (panel (b)) approaches. The central red dot represents the mean of the errors, whereas top and bottom edges show the standard deviation (SD) for all the patients. The central black dotted horizontal line represents a reference at '0'.

Table 6
Relative errors R_r using stage-specific (S) and patient-specific (P) approaches for the multivariable estimator.

R_r	h_0	h_1	h_2	h_3	h_{48}
S	0.011 ± 0.442	0.000 ± 0.315	−0.001 ± 0.234	−0.002 ± 0.201	−0.008 ± 0.347
P	0.163 ± 0.348	−0.058 ± 0.194	−0.042 ± 0.184	−0.065 ± 0.142	0.085 ± 0.246

*Values are expressed as mean ± standard deviation.

Table 7
Intra-patient pearson correlation coefficients (r) between actual and estimated $[K^+]$ ($r_{[K^+],[K^+]_e}$) using stage-specific (S) and patient-specific (P) approaches for univariable and multivariable estimators.

$r_{[K^+],[K^+]_e}$	η	d_w	η, d_w
S	0.98 (0.03)	0.97 (0.06)	0.97 (0.05)
P	0.32 (1.29)	0.65 (1.07)	0.77 (0.88)

*Values are expressed as median (IQR).

correlation coefficient between actual and estimated $[K^+]$ for univariable and multivariable estimators using stage-specific and patient-specific approaches.

Bland-Altman plots between actual and estimated $[K^+]$ for the proposed markers are shown in Supplementary Material (Figs. S3–S7).

A comparison between estimation errors obtained for T wave markers analyzed in the present study and in previous studies is presented in Tables 8–9.

4. Discussion

We analyzed the T waves of the ECG in ESRD patients during and after HD by nonlinear dynamics and morphology markers. Three nonlinear dynamics markers were evaluated: the first two, λ^t and λ^{wt}, assessed repolarization instabilities and temporal inter-beat variability by computing the maximum Lyapunov exponent from T wave sequences before and after warping, respectively; the third one, η, was proposed in this study to measure intra-beat differences in an averaged representative T wave after subtraction of a reference wave. Additionally, three warping-based markers were evaluated to assess morphological variability in the time domain (d_w) and amplitude domain (d_a and d_a^{NL}). A comparison between our investigated markers and previously proposed markers, $T_{S/A}$ [25,26] and $T_{S/\sqrt{A}}$ [23], was performed. The correlation between the analyzed T wave markers and serum $[K^+]$ during and after HD was found to be particularly strong for η and d_w. ECG estimators of $[K^+]$ were built based on individual and combined values of these two markers. We found a tight relationship between actual and estimated $[K^+]$ values, especially when the estimation used population ECG data evaluated at the same time stage after the start of an HD session. Our

Table 8
Estimation errors (ε) for T wave markers and their combinations using stage-specific (S) estimators.

$\varepsilon(S)$	h_0	h_1	h_2	h_3	h_{48}
$T_{S/A}$	0.019 ± 1.159	0.620 ± 0.517	0.003 ± 0.630	0.004 ± 0.559	0.007 ± 0.730
$T_{S/\sqrt{A}}$	0.009 ± 1.180	−0.001 ± 0.825	0.003 ± 0.627	0.001 ± 0.554	0.003 ± 0.947
d_w	0.010 ± 1.132	0.012 ± 0.845	0.008 ± 0.636	0.009 ± 0.543	−0.032 ± 0.919
η	0.016 ± 1.221	−0.006 ± 0.847	−0.009 ± 0.621	−0.010 ± 0.574	0.005 ± 0.996
d_w and η	0.030 ± 1.225	−0.001 ± 0.874	−0.002 ± 0.648	−0.006 ± 0.556	−0.023 ± 0.960

*Values are expressed as mean ± standard deviation and the units are mM.

Table 9
Estimation errors (ε) for T wave markers and their combinations using patient-specific (P) estimators.

$\varepsilon(P)$	h_0	h_1	h_2	h_3	h_{48}
$T_{S/A}$	0.967 ± 0.729	0.479 ± 0.455	0.357 ± 0.350	0.381 ± 0.409	0.922 ± 1.192
$T_{S/\sqrt{A}}$	0.904 ± 1.413	0.022 ± 0.827	−0.248 ± 0.299	−0.333 ± 0.402	0.353 ± 1.373
d_w	0.665 ± 0.981	−0.202 ± 0.533	−0.143 ± 0.540	−0.282 ± 0.418	0.407 ± 0.582
η	0.831 ± 0.802	−0.287 ± 0.525	−0.435 ± 0.318	−0.390 ± 0.419	0.530 ± 0.672
d_w and η	0.451 ± 0.964	−0.161 ± 0.539	−0.116 ± 0.508	−0.180 ± 0.392	0.235 ± 0.681

*Values are expressed as mean ± standard deviation and the units are mM.

results can be used for noninvasive monitoring of $[K^+]$ in ESRD patients to anticipate arrhythmic risk associated with hypo- or hyperkalemia.

4.1. T waves variations during and after HD

This study investigated maximum Lyapunov exponent-based markers to characterize changes in the T wave of the ECG and their association with serum electrolyte levels. Previous studies have investigated indices of repolarization instability in patients undergoing HD, including T wave alternans [40], beat-to-beat QT interval variability [13] or T wave periodic repolarization dynamics [41]. However, most of these studies either have not been able to establish a clear correlation between the values of the evaluated indices and serum potassium levels or have reported moderate correlation coefficients, thus limiting their possibilities for ambulatory $[K^+]$ monitoring. We assessed whether nonlinear dynamics of the T wave could help in capturing relevant information on the changes in repolarization characteristics during and after HD. Also, on the basis of recent studies where we measured T wave morphological variability by time warping-based techniques and we showed its tight relationship with $[K^+]$, we investigated the combination of nonlinear dynamics and morphology descriptors to improve their individual performances for $[K^+]$ monitoring.

To characterize nonlinear dynamics we evaluated the maximum Lyapunov exponent from 2-min sequences of T waves taken every hour from the start of HD and 48 h after it. Lyapunov exponents quantify the sensitivity of a dynamical system to the initial conditions by measuring how a small change in the system variables at a certain time affects the behavior of the system at a future time [36]. Here, we calculated λ^t and λ^{wt}, representing the maximum Lyapunov exponent from unwarped and warped T wave sequences, respectively, and we found them to take positive values at all evaluated stages during and after HD. These results would indicate chaotic behavior in the form of local repolarization instabilities, which are significantly larger at the onset of the HD sessions when $[K^+]$ is elevated.

Also, we investigated a novel marker, η, evaluated from inter-MWTWs computed during and after HD to describe intra-beat dissimilarities and their variations with $[K^+]$. We found η to take higher values at the beginning of HD sessions, which would point to larger intra-beat differences in repolarization associated with raised $[K^+]$. This is concordant with the fact that T wave amplitude increases with $[K^+]$ and so does its difference with respect to the reference T wave.

To confirm the robustness of our calculations, we varied the values of the parameters used in the definition of λ^t, λ^{wt} and η and found relatively modest effects around the default parameter values as compared to changes measured during HD, particularly for η. To assess the specific information captured by the investigated nonlinear dynamics markers, we generated synthetic T waves and showed that λ^t and λ^{wt} mainly reflected temporal inter-beat variability while η was more sensitive to simulated amplitude and duration modulations.

4.2. Correlation of T wave changes markers to [K$^+$]

The correlation with [K$^+$] was particularly strong for the nonlinear dynamics marker η and the time-domain morphological variability marker d_w, with median Pearson correlation coefficients across patients above 0.78. Importantly, the relationship between each of these two markers and [K$^+$] remained tight even after removal of the effects of covariates like heart rate, with partial linear correlation coefficients still above 0.78. Such a relationship was, however, weaker when the effects of [Ca^{2+}] were removed. This could be explained by [K$^+$] and [Ca^{2+}] exerting concurrent changes in the T wave during HD.

Previous works have shown that the T wave of the ECG is altered by variations in [K$^+$] [3,9–11], with narrow and peaked T waves recorded under high levels of [K$^+$] [2,3,5,42], in agreement with our observations. The effects of [K$^+$] on specific T wave features like width, amplitude, slope, slope-to-amplitude or amplitude-to-slope ratio have been quantified [25–27,43,44]. Some of these features are very sensitive to T wave delineation and thus could be more prone to errors when measured in ambulatory recordings. Other markers, like the slope-to-amplitude, were tested in a previous study of us and were found to present changes that were as strongly correlated to [K$^+$] variations as the time-domain morphology marker d_w, both with and without removing the effects of other covariates like heart rate and [Ca^{2+}] [28].

Morphological characteristics of the T wave have been evaluated in previous studies, as recently reviewed [11]. In particular, a morphology combination score (MCS) based on T wave asymmetry, flatness and notching [45,46] has been used to analyze the relationship between changes in the T wave shape and [K$^+$] variations in large scale populations [47]. A strong correlation was found between MCS and [K$^+$] when the latter varied in the range 2–4.1 mM but not in the range 4.2–6 mM. Our proposed markers of T wave morphological variability were strongly correlated with [K$^+$] in a wide range of values, including both hypo- and hyperkalemic values. For some of our morphology markers, such a relationship was better represented by a nonlinear function than by a linear one [30], which agrees with previous studies describing nonlinear relationships between T wave markers like the slope-to-amplitude ratio and [K$^+$] [26] and could help to explain the lower linear correlations found in other studies investigating [K$^+$]-induced alterations in ECG repolarization.

Mathematical modeling and numerical simulation have been used as tools to provide mechanistic understanding of ECG changes elicited in response to electrolyte variations and to improve the processing methods used to derive ECG markers with capacity for [K$^+$] monitoring [11,26,48,49]. In the case of T wave morphology markers, *in silico* analysis has been used to explain the high inter-individual variation in patterns measured in ESRD patients with varying [K$^+$] [28,50]. Differences in transmural distributions of endocardial, midmyocardial and epicardial cells contributed to explain the inter-individual variability in the T wave response to [K$^+$] variations. In the case of T wave nonlinear dynamics, this is the first study investigating the markers λ^t, λ^{wt} and η and their relationship to [K$^+$]. Similarly to the morphological markers, we observed large inter-individual differences in nonlinear dynamics characteristics. Our work on synthetic T waves simulating linear and nonlinear amplitude and duration changes served to establish the effects captured by these indices, with different levels of temporal inter-beat variability having a direct effect on their magnitudes, as discussed in the previous section.

4.3. Estimation of [K$^+$] from T wave markers

Taking the two markers presenting the highest correlation with [K$^+$], i.e. η and d_w, we designed ECG-based [K$^+$] estimators. On top of univariable estimators using one of these two markers, we built multivariable estimators based on their combination. For each of the constructed estimators, we considered both stage-specific and patient-specific

approaches, with the first approach estimating [K$^+$] for a patient at a given HD stage based on population data measured at the same stage with respect to the start of an HD session and the second approach estimating [K$^+$] for a patient at a given time stage based on data from the same patient measured at different time stages. The stage-specific approach rendered results that were unbiased in mean and median over patients. However, the dispersion was generally larger than for the patient-specific approach. The combination of the two markers η and d_w led to overall improvements in terms of reduced estimation errors (Fig. 11 and Table 9). Multivariable [K$^+$] estimates also correlated significantly better with actual [K$^+$] than univariable estimates in the patient-specific approach. Agreement between actual and estimated [K$^+$] was promising using our proposed T wave markers as compared to previously proposed T wave markers [23,25,26], which was confirmed by Bland-Altman analysis and calculation of estimation errors. The estimation errors over patients and HD stages using the patient-specific approach were 0.046 ± 0.69 mM for the combination of η and d_w, while they were 0.091 ± 0.96 mM for $T_{S/A}$ and 0.139 ± 1.07 mM for $T_{S/\sqrt{A}}$. Also, we confirmed the suitability of [K$^+$] estimation based on our ECG proposed markers under synthetic noisy scenarios, in which we took the ECG signal of a patient and we added noise at signal-to-noise ratio (SNR) values down to 5 dB. Estimation errors (ε) based on d_w and η were, in median over HD points, always below 0.4 mM, while these reached 0.73 mM for $T_{S/A}$ at the lowest SNRs (Fig. S8 in Supplementary Material).

The highest estimation errors were obtained at the start of the HD session (h_0) and 48 h after it (h_{48}), corresponding to the highest [K$^+$] values. The reason for this could lie in the fact that these HD stages are associated with [K$^+$] values well apart from the ones measured at h_1, h_2, h_3 and h_4, which translates into large differences in the T wave markers at h_0 and h_{48} as compared to other HD points. In the learning phase, the estimators are fitted to all the available values along and after HD, with large relevance of the high number of HD stages corresponding to lower [K$^+$], which would explain the lower performance of the estimators at h_0 and h_{48}. Future research could be designed so as to have more available [K$^+$] measurements during the time period from the end of the HD session to the start of a new session 48 h later, or during the first hour of the HD. This would allow improved learning of the estimators, which could also be designed to account for nonlinear relationships between the investigated repolarization markers and [K$^+$]. Previous studies have shown the relevance of accounting for such nonlinearities in the design of the estimators [26,30], which we discarded in the present study due to the limited number of sampled HD stages per patient.

The above discussed results suggest that T wave nonlinear dynamics and warping-based morphology markers have value for [K$^+$] monitoring during inter-dialytic periods in ESRD patients.

4.4. Study limitations and future research

This study analyzed 48-h ECG recordings of 29 ESRD patients. Future studies including a larger number of patients and more frequent blood samples during the inter-dialytic period would allow to confirm the present findings and extend the investigation to ECG-based nonlinear estimators of [K$^+$].

We focused our research on the effects of [K$^+$] on ventricular repolarization. The impact of other electrolytes like [Ca^{2+}] and [Mg^{2+}] could also be analyzed and univariable and multivariable estimators could be derived from ECGs. While some reports have already described alterations in T wave morphology in response to variations in [Ca^{2+}] and [Mg^{2+}] [10,20,51–53], the impact on T wave nonlinear dynamics remains unknown.

Other multivariable estimators including indices reported in previous studies [23–26,54] could be tested to analyze its potential for improved noninvasive monitoring of [K$^+$].

The present work could be extended to include deep learning-based approaches for serum electrolyte estimation provided large data sets of

ECG recordings and concomitant blood samples were available for the analysis, in line with studies already addressing hypo- and hyperkalemia screening from the ECG using deep learning methods [55–57].

5. Conclusions

Noninvasive monitoring of $[K^+]$ in ESRD patients based on combined T wave nonlinear dynamics and morphological variability markers is feasible. The proposed methods can find application in hypo- and hyperkalemia screening, which can be of major relevance to anticipate arrhythmic events in these patients.

Declaration of interests

The authors declare that they have no known competing financial interests or personal relationships that could have appeared to influence the work reported in this paper.

Acknowledgment

Appendix A. Supplementary data

Supplementary data to this article can be found online at https://doi.org/10.1016/j.compbiomed.2022.105304.

References

[1] N.R. Hill, et al., Global prevalence of chronic kidney disease - a systematic review and meta-analysis, PLoS One 11 (7) (2016), e0158765.

[2] J.N. Weiss, et al., Electrophysiology of hypokalemia and hyperkalemia, Circ. Arrhythm. Electrophysiol. 10 (3) (2017).

[3] N. El-Sherif, G. Turitto, Electrolyte disorders and arrhythmogenesis, Cardiol. J. 18 (3) (2011) 233–245.

[4] J. Soar, et al., European Resuscitation Council Guidelines for Resuscitation 2010 Section 8. Cardiac arrest in special circumstances: electrolyte abnormalities, poisoning, drowning, accidental hypothermia, hyperthermia, asthma, anaphylaxis, cardiac surgery, trauma, pregnancy, electrocution, Resuscitation 81 (10) (2010) 1400–1433.

[5] J.T. Levis, ECG diagnosis: hypokalemia, Perm. J. 16 (2) (2012) 57.

[6] M. Kanbay, et al., Sudden death in hemodialysis: an update, Blood Purif. 30 (2) (2010) 135–145.

[7] H. Bozbas, et al., Prevalence and predictors of arrhythmia in end stage renal disease patients on hemodialysis, Ren. Fail. 29 (3) (2007) 331–339.

[8] A. Lanari, et al., Electrocardiographic effects of potassium. I. Perfusion through the coronary bed, Am. Heart J. 67 (3) (1964) 357–363.

[9] C. Van Mieghem, et al., The clinical value of the ECG in noncardiac conditions, Chest 125 (4) (2004) 1561–1576.

[10] R. Noordam, et al., Effects of calcium, magnesium, and potassium concentrations on ventricular repolarization in unselected individuals, J. Am. Coll. Cardiol. 73 (24) (2019) 3118–3131.

[11] N. Pilia, et al., Quantification and classification of potassium and calcium disorders with the electrocardiogram: what do clinical studies, modeling, and reconstruction tell us? APL Bioengineering 4 (4) (2020), 041501.

[12] B. Di Iorio, A. Bellasi, QT interval in CKD and haemodialysis patients, Clin. Kidney J. 6 (2) (2013) 137–143.

[13] M.R. Khosoosi Niaki, et al., Changes in QT interval before and after hemodialysis, Caspian J. Intern. Med. 4 (1) (2013) 590–594.

[14] P.M. Sohal, et al., Effect of hemodialysis on corrected QT interval and QTc dispersion, Indian J. Nephrol. 28 (5) (2018) 335–338.

[15] Y. Matsumoto, et al., Changes in QTc interval in long-term hemodialysis patients, PLoS One 14 (1) (2019), e0209297.

[16] M. Malhis, et al., Changes in QT intervals in patients with end-stage renal disease before and after hemodialysis, Saudi J. Kidney Dis. Transpl. 21 (3) (2010) 460–465.

[17] E.D. Kim, et al., Associations of serum and dialysate electrolytes with QT interval and prolongation in incident hemodialysis: the predictors of arrhythmic and cardiovascular risk in end-stage renal disease (PACE) study, BMC Nephrol. 20 (1) (2019) 133.

[18] I. Lorincz, et al., QT dispersion in patients with end-stage renal failure and during hemodialysis, J. Am. Soc. Nephrol. 10 (6) (1999) 1297–1302.

[19] A. Covic, et al., Haemodialysis increases QTc interval but not QTc dispersion in ESRD patients without manifest cardiac disease, Nephrol. Dial. Transplant. 17 (12) (2002) 2170–2177.

[20] H. Ozportakal, et al., Hemodialysis-induced repolarization abnormalities on ECG are influenced by serum calcium levels and ultrafiltration volumes, Int. Urol. Nephrol. 49 (3) (2017) 509–515.

[21] S. Severi, et al., Cardiac response to hemodialysis with different cardiovascular tolerance: heart rate variability and QT interval analysis, Hemodial. Int. 10 (3) (2006) 287–293.

[22] F. Floccari, et al., QTc interval and QTc dispersion during haemodiafiltration, Nephrology 9 (6) (2004) 335–340.

[23] Z.I. Attia, et al., Novel bloodless potassium determination using a signal-processed single-lead ECG, J. Am. Heart Assoc. 5 (1) (2016).

[24] S. Severi, et al., Noninvasive potassium measurements from ECG analysis during hemodialysis sessions, in: 2009 36th Annual Computers in Cardiology Conference, CinC, 2009, pp. 821–824.

[25] C. Corsi, et al., Validation of a novel method for non-invasive blood potassium quantification from the ECG, in: 2012 Computing in Cardiology, 2012, pp. 105–108.

[26] C. Corsi, et al., Noninvasive quantification of blood potassium concentration from ECG in hemodialysis patients, Sci. Rep. 7 (2017) 42492.

[27] J.J. Dillon, et al., Noninvasive potassium determination using a mathematically processed ECG: proof of concept for a novel "blood-less, blood test, J. Electrocardiol. 48 (1) (2015) 12–18.

[28] H.A. Bukhari, et al., Characterization of T wave amplitude, duration and morphology changes during hemodialysis: relationship with serum electrolyte levels and heart rate, IEEE (Inst. Electr. Electron. Eng.) Trans. Biomed. Eng. (2020), 1–1.

[29] F. Palmieri, et al., Monitoring blood potassium concentration in hemodialysis patients by quantifying T-wave morphology dynamics, Sci. Rep. 11 (1) (2021) 3883.

[30] F. Palmieri, et al., Nonlinear T-wave time warping-based sensing model for non-invasive personalized blood potassium monitoring in hemodialysis patients, Sensors 21 (2710) (2021) 1–13.

[31] L. Li, et al., Physiological signal variability analysis based on the largest Lyapunov exponent, in: 2009 2nd International Conference on Biomedical Engineering and Informatics, 2009, pp. 1–5.

[32] S. Srinivasan, et al., Analysis of T wave nonlinear dynamics for serum potassium monitoring in end-stage renal disease patients, in: 2020 Computing in Cardiology, 2020, pp. 1–4.

[33] J.P. Martínez, et al., A wavelet-based ECG delineator: evaluation on standard databases, IEEE Trans. Biomed. Eng. 51 (4) (2004) 570–581.

[34] F. Castells, et al., Principal component analysis in ECG signal processing, EURASIP J. Appl. Signal Process. 2007 (1) (2007) 1–21.

[35] J. Ramirez, et al., Variability of ventricular repolarization dispersion quantified by time-warping the morphology of the T-waves, IEEE Trans. Biomed. Eng. 64 (7) (2017) 1619–1630.

[36] M.T. Rosenstein, et al., A practical method for calculating largest Lyapunov exponents from small data sets, Physica D 65 (1) (1993) 117–134.

[37] R. Killick, et al., Optimal detection of changepoints with a linear computational cost, J. Am. Stat. Assoc. 107 (500) (2012) 1590–1598.

[38] R.A. Fisher, Statistical methods for research workers, in: S. Kotz, N.L. Johnson (Eds.), *Breakthroughs in Statistics: Methodology and Distribution*, Ser. Springer Series in Statistics, 1992, pp. 66–70. New York, NY.

[39] J.M. Bland, D.G. Altman, Statistical methods for assessing agreement between two methods of clinical measurement, Lancet (London, England) 1 (8476) (1986) 307–310.

[40] E.A. Secemsky, et al., High prevalence of cardiac autonomic dysfunction and T-wave alternans in dialysis patients, Heart Rhythm 8 (4) (2011) 592–598.

[41] D. Schüttler, et al., Large potassium shifts during dialysis enhance cardiac repolarization instability, J. Nephrol. (2020).

[42] C. Slovis, R. Jenkins, ABC of clinical electrocardiography: conditions not primarily affecting the heart, BMJ 324 (7349) (2002) 1320–1323.

[43] S. Kharche, et al., Simulating the effects of serum potassium on the ECG, in: 2012 Computing in Cardiology, 2012, pp. 225–228.

[44] P.P. Frohnert, et al., Statistical investigation of correlations between serum potassium levels and electrocardiographic findings in patients on intermittent hemodialysis therapy, Circulation 41 (4) (1970) 667–676.

[45] M. Andersen, et al., A robust method for quantification of IKr-related T-wave morphology abnormalities, in: 2007 Computers in Cardiology, 2007, pp. 341–344.

[46] S.G. Tischer, et al., Influence of type of sport on cardiac repolarization assessed by electrocardiographic T-wave morphology combination score, J. Electrocardiol. 51 (2) (2018) 296–302.

[47] M.L. Krogager, et al., The relationship between serum potassium concentrations and electrocardiographic characteristics in 163,547 individuals from primary care, J. Electrocardiol. 57 (2019) 104–111.

[48] S. Severi, et al., Calcium and potassium changes during haemodialysis alter ventricular repolarization duration: in vivo and in silico analysis, Nephrol. Dial. Transplant. 23 (4) (2008) 1378–1386.

[49] M. Hernández Mesa, et al., Effects of serum calcium changes on the cardiac action potential and the ECG in a computational model, Curr. Dir. Biomed. Eng. 4 (1) (2018) 251–254.

[50] H.A. Bukhari, et al., Transmural ventricular heterogeneities play a major role in determining T-wave morphology at different extracellular potassium levels, in: 2019 Computing in Cardiology, CinC, 2019, pp. 1–4.

[51] N. Naksuk, et al., Association of serum magnesium on mortality in patients admitted to the intensive cardiac care unit, Am. J. Med. 130 (2) (2017) 229. e5–229.e13.

[52] W.K. Jhang, et al., Severe hypermagnesemia presenting with abnormal electrocardiographic findings similar to those of hyperkalemia in a child undergoing peritoneal dialysis, Korean J. Pediatr. 56 (7) (2013) 308–311.

[53] W.M. van den Bergh, et al., Electrocardiographic abnormalities and serum magnesium in patients with subarachnoid hemorrhage, Stroke 35 (3) (2004) 644–648.

[54] O.Z. Yasin, et al., Noninvasive blood potassium measurement using signal-processed, single-lead ecg acquired from a handheld smartphone, J. Electrocardiol. 50 (5) (2017) 620–625.

[55] C.-S. Lin, et al., A deep-learning algorithm (ECG12Net) for detecting hypokalemia and hyperkalemia by electrocardiography: Algorithm development, JMIR Med. Inform. 8 (3) (2020).

[56] C.D. Galloway, et al., Development and validation of a deep-learning model to screen for hyperkalemia from the electrocardiogram, JAMA Cardiol 4 (5) (2019) 428–436.

[57] J. Kwon, et al., Artificial intelligence for detecting electrolyte imbalance using electrocardiography, Ann. Noninvasive Electrocardiol. 26 (3) (2021), e12839.